**Atmospheric
Chemistry
and Physics
Discussions**

Atmospheric diurnal and semi-diurnal variations observed with GPS radio occultation soundings

F. Xie[1,*], D. L. Wu[1], C. O. Ao[1], and A. J. Mannucci[1]

[1]Jet Propulsion Laboratory, California Institute of Technology, Pasadena, California, USA
[*]now at: Joint Institute for Regional Earth System Science and Engineering (JIFRESSE), University of California, Los Angeles, California, 90095, USA

Correspondence to: F. Xie (feiqin.xie@jpl.nasa.gov)

ACPD

9, 25409–25441, 2009

Atmospheric diurnal and semi-diurnal variations observed with GPS soundings

F. Xie et al.

Title Page

Abstract	Introduction
Conclusions	References
Tables	Figures

|◄ | ►|
◄ | ►

Back | Close

Full Screen / Esc

Printer-friendly Version

Interactive Discussion

Abstract

Diurnal and semi-diurnal variations, driven by solar forcing, are two fundamental modes in the Earth's weather and climate system. Radio occultation (RO) measurements from the six COSMIC satellites (Constellation Observing System for Meteorology Ionosphere and Climate) provide rather uniform global coverage with high vertical resolution, all-weather and diurnal sampling capability. This paper analyzes the diurnal and semi-diurnal variations of both temperature and refractivity from two-year (2007–2008) COSMIC RO measurements in the troposphere and stratosphere. The RO observations reveal both propagating and trapped vertical structures of diurnal and semi-diurnal variations, including transition regions near the tropopause where data with high vertical resolution are critical. In the tropics the diurnal amplitude in refractivity decreases with altitude from a local maximum in the planetary boundary layer and reaches the minimum around 14 km and then further increase amplitude in the stratosphere. The upward propagating component of the migrating diurnal tides in the tropics is clearly captured by the GPS RO measurements, which show a downward progression in phase from upper troposphere to the stratopause with a vertical wavelength of about 25 km. Below 500 hPa (∼5.5 km), seasonal variations of the peak diurnal amplitude in the tropics follow the solor forcing change in latitude, while at 30 km the seasonal pattern reverses with the diurnal amplitude peaking at the opposite side of the equator relative to the solar forcing. Polar regions shows large diurnal variations in the stratosphere with strong seasonal variations and the cause(s) of these variations require further investigations.

1 Introduction

Driven by the persistent daily solar heating, the diurnal cycle is one of the fundamental variations in the Earth's weather and climate system, which modulates dynamical, hydrological, radiative, and chemical processes throughout the atmosphere.

Observations of the diurnal variation can be found in numerous atmospheric variables. Near the ground, weather reports show that surface air temperature, pressure, winds, precipitation (Dai and Deser, 1999; Dai et al., 1999) and precipitable water vapor (Dai et al., 2002) vary greatly in 24 h. In the troposphere, satellite radiances measurements re-
5 veal a significant diurnal cycle of hydrological processes in terms of precipitation (Nesbitt and Zipser, 2003), deep convection, cloudiness and upper tropospheric humidity (UTH) (e.g. Tian et al., 2004, 2005; Chung et al., 2007). In the upper troposphere and above, up to the mesosphere and thermosphere, the propagating tidal waves from the water vapor and ozone heating have been extensively investigated and described in
10 the monograph by Chapman and Linzen (1970). The latest observations of the tidal waves can be found in radiosonde sounding (Tsuda et al., 1994, Huang et al., 2009), lidar (e.g. Williams et al., 1998; States and Gardner, 2000; She et al., 2002), radar (e.g. Tsuda et al., 1988), and satellite observations (e.g. Hays et al., 1994; McLandress et al., 1996; Wu et al., 1998; Zeng et al., 2008).
15 The atmospheric diurnal cycle is a process that must be represented realistically in global and regional models for numerical weather and climate prediction, but there is still lack of a thorough understanding of physical mechanisms and processes from the planetary boundary layer (PBL) as well as in the troposphere in these models (e.g. Slingo et al., 1987; Randall et al., 1991; Lin et al., 2000; Yang and Slingo, 2001;
20 Betts and Jakob, 2002; Dai and Trenberth, 2004; Tian et al., 2004). Poor representation of the diurnal cycle in the climate model could lead to systematic biases in the mean climate (Keckhut et al., 2001; Neale and Slingo, 2003). In addition, sampling the diurnal cycle is also critical for detecting and monitoring subtle trends in climate change (Dai, 1999).
25 Characterizing and understanding the atmospheric diurnal cycle requires measurements with sufficient spatial and temporal resolutions for both regional and global studies. Conventional satellite observations (e.g. passive infrared and microwave sounder) provide high spatial and temporal resolution atmospheric measurements but with relatively poor vertical resolution and accuracy. Despite high vertical resolution

measurements in the troposphere and lower stratosphere from radiosondes, temperature and wind in the mesosphere and lower thermosphere from lidars and radars, such measurements are limited in terms of geographical and temporal coverage.

Atmospheric profiling with the GPS Radio Occultation (RO) emerges as a relatively new technique to provide high-precision temperature and water vapor measurements with global coverage and high vertical resolution (~200 m in the troposphere to ~1 km in the stratosphere). Insensitive to clouds and precipitation, GPS RO measurements are especially valuable for studying the diurnal variation in the troposphere (Kursinski et al., 1997). Zeng et al. (2008) studied the diurnal temperature variation in the tropics using GPS/CHAMP (CHAllenging Minisatellite Payload) observations during 2001–2005. Because CHAMP is a polar-orbiting satellite and precesses slowly, it takes roughly 90-day to fully sample a diurnal cycle (Pirscher et al., 2007; Zeng et al., 2008). Due to a slow variation in the equatorial diurnal tide, Zeng et al. (2008) assumed that the diurnal tide was invariant during the CHAMP diurnal sampling period and was able to extract vertical, seasonal, and latitudinal structures of the migrating component of the tide from a composite of 51-month CHAMP temperature profiles at altitudes of 10–30 km. However, their diurnal analysis was limited to the temperature data, not including the lower troposphere and upper stratosphere.

Since its launch in April 2006, the six-satellite constellation COSMIC (Constellation Observing System for Meteorology Ionosphere and Climate) RO mission yields rather dense sampling (over 2000 profiles per day) around the globe (Anthes et al., 2008). More importantly, the open-loop tracking receivers on all COSMIC satellites have significantly improved the RO sounding capability by acquiring a large number of measurements at the PBL altitudes (Sokolovskiy et al., 2006; Ao et al., 2009). In the past, high water vapor variability prevented the close-loop receiver (such as one equipped on CHAMP and many others) from properly tracking the GPS transmitter signals, resulting in retrieval failure and large bias in the lower troposphere (Ao et al., 2003; Beyerle et al., 2003). Like the CHAMP orbit, the COSMIC satellite orbits precess with time. However, with the six satellites, the full diurnal cycle can be sampled well within one month

Atmospheric diurnal and semi-diurnal variations observed with GPS soundings

F. Xie et al.

◄◄ | ►►

◄ | ►

Back | Close

Full Screen / Esc

Printer-friendly Version

Interactive Discussion

on a global basis. By December 2006, six satellites were spread out far enough in local time coverage to yield a nearly complete diurnal sampling, and the orbit configuration in 2007 further matures for the diurnal study. Each single COSMIC satellite (in final orbit) has a drifting rate of about $-2°$/day, relative to the Earth's mean motion of about $+1°$/day. Thus, the six satellites, with a 30° orbital plane spacing, give a full diurnal cycle sampling within 10 days at low and midlatitudes and within about one month for higher latitudes (Pirscher et al., 2007).

In this study, we analyze two-year (2007–2008) of COSMIC RO soundings to derive vertical structures of the diurnal variation of temperature and refractivity at altitudes from the PBL to the upper stratosphere. Section 2 describes the COSMIC dataset and the harmonic analysis method to extract the diurnal signals. In Sect. 3, the diurnal amplitude and phase of the migrating tide in the tropics are analyzed and compared to other observations and the well-established tidal wave theory. We further extend our analysis to the global RO soundings, and present time series and zonal-mean structures of the diurnal and semidiurnal amplitude of the RO refractivity from PBL to the upper stratosphere in Sects. 4–5. Discussions, conclusions and future work can be found in Sects. 6–7.

2   Data sampling and analysis

2.1   GPS Radio Occultation (RO) sounding technique

GPS RO technique senses the atmosphere by receiving the GPS radio signals at two L-band frequencies (L1~1.6 GHz and L2~1.2 GHz) from a moving LEO (Low Earth Orbit) satellite receiver. As the LEO receiver sets behind the horizon relative to the transmitting GPS satellite, the radio wave is refracted (or bent) and its travel time is delayed due to variations of refractivity. The basic measurements in GPS RO are the time series of GPS carrier phase and signal amplitude recorded at the LEO receiver. From the precise determination of the GPS orbits and the location of the receiver, the excess

phase, defined as the difference between the measured phase and that predicted for a vacuum, is also accurately calculated and corrected for GPS and receiver clock errors. The excess phase and amplitude are then used to derive the bending angle as a function of tangent height, from which the refractivity profile can be retrieved from the top of the atmosphere to the lower atmosphere with the so-called onion-peeling approach. Then the temperature and humidity profiles can be further derived from the refractivity (Kursinski et al., 1997; Rocken et al., 1997). Extensive validation and evaluation of the precision and accuracy of the RO measurements against other observations and models have been carried out by many authors (e.g. Kuo et al., 2004; Shreiner et al., 2007).

In the neutral atmosphere, the refractivity, N, a dimensionless quantity defined as $N=(n-1)\times10^6$, where n is the refractive index, is related to the atmospheric pressure (P in mbar), temperature (T in Kelvin), and water vapor partial pressure (P_w in mbar) through (Smith and Weintraub, 1953).

$$N=b_1\frac{P}{T}+b_2\frac{P_w}{T^2}, \tag{1}$$

where $b_1=77.6\,\mathrm{K\,hPa^{-1}}$ and $b_2=3.73\times10^5\mathrm{K^2\,hPa^{-1}}$. The refractivity profile can be retrieved from the bending angle profile from near the surface up to $\sim$60 km before the measurements become too noisy. The moisture contribution to the refractivity can be neglected at altitudes above $\sim$8 km (in the tropics) where the water vapor volume mixing ratio is usually less than 10^{-4} (Kursinski, et al, 1997), In this case, Eq. (1) is reduced to:

$$N=b_1\frac{P}{T}=(b_1\cdot R)\cdot\rho=k\cdot\rho \tag{2}$$

where the gas constant $R=287\,\mathrm{J\,kg^{-1}\,K^{-1}}$, $k=b_1\cdot R=222.71\,\mathrm{J\,kg^{-1}\,Pa^{-1}}$, and ρ is density of the atmosphere that is proportional to the refractivity. So the pressure can be obtained from density (or refractivity) by integrating the hydrostatic equilibrium equation. The integration starts from a pressure level high in the atmosphere with an a priori

temperature guess. The initial pressure error due to the temperature guess decreases rapidly as integration moves deeper into the atmosphere (Kursinski et al., 1997). The temperature can then be inferred via Eq. (2) with the dry atmosphere assumption, which can be generally hold throughout the stratosphere and the cold upper tropo-
5 sphere with temperature less than 250 K. The retrieval is switched to moisture retrieval where temperature is greater than 250 K. In the moisture retrieval, the pressure and water vapor pressure can be derived given an a priori temperature profile, which is usually obtained from global analysis data (Hajj et al., 2002). Alternatively, humidity and temperature can be retrieved simultaneously using 1-D variational analysis provided the
10 background information from model analysis (Healy and Eyre, 2000; Kursinski et al., 2000; Poli and Kursinski, 2002).

In the moist troposphere, the refractivity is a weighted sum of dry air density and water vapor density, and thus affected by both temperature and water vapor pressure. As shown in Fig. 6f of Xie et al. (2008) based on a mid-latitude radiosonde profile,
15 the solely 1 K perturbation of temperature corresponds to ~0.4% refractivity change at all altitudes. On the other hand, the derivative of refractivity with respective to specific humidity depends on the amount of water vapor, which is a strong function of height. Roughly speaking, a 1 g/kg change in specific humidity q corresponds to ~2.5% change in refractivity but can vary slightly with temperature. For example, inside a well-
20 mixed PBL where specific humidity is about q=8 g/kg, the ratio is ~2.2%/(g/kg); at the top of the PBL, around 1.8 km, where q=3 g/kg, the ratio is 2.7%/(g/kg); in the middle troposphere (~5 km), where q=0.8 g/kg, the ratio is ~3%/(g/kg).

2.2 COSMIC RO data and sampling

In this study, we use COSMIC RO level-2 refractivity and temperature data in 2007–
25 2008 as retrieved at NASA Jet Propulsion Laboratory (JPL) (Hajj et al., 2002; Ao et al., 2009). The retrieved profiles are reported as a function of geometric height above mean-sea-level (MSL). COSMIC acquires about 2000 occultations a day, however, the number of valid RO profiles reduces after the calibration and quality control procedure.

The current JPL retrieval applies double differencing calibration, which has resulted in a large percentage of calibration failure due to the lack of required ground reference station data. Meanwhile, a relatively stringent quality-control procedure (e.g. RO profiles with temperature over 10 K apart from ECMWF analysis or with refractivity over 10% apart from ECMWF at any altitude below 40 km will be removed) further reduces the sampling (especially over polar region, where large temperature variation due to planetary waves and gravity waves might not resolved by the model) by about 25% (Ho et al., JGR, 2009). A total of 641, 134 valid profiles over the two-year span (2007~2008) have been used in this study.

The JPL temperature retrievals are scientifically useful at height range from ~8 km (in the tropics) to ~40 km. The upper boundary is limited by the measurement noise (Kursinski et al., 1997) whereas the lower boundary is limited by the ambiguity of temperature and water vapor that is inseparable in the upper troposphere. At higher latitudes, temperature retrievals can be available down to the boundary layer during winter months. On the other hand, the refractivity measurement is useful at a much greater height range (0–50 km) but requires careful interpretation to connect to atmospheric physical quantities. Therefore, in the following sections, besides the RO temperature, refractivity profiles are also used to demonstrate the vertical structure of atmosphere diurnal variation for the whole neutral atmosphere across the globe.

2.3 Linear harmonic analysis method

The JPL temperature and refractivity retrievals are output at ~50 m and ~400 m interval vertically at altitudes below and above 20 km, respectively. In this study, we interpolate (with cubic spline) each profile onto 50 standard vertical pressure levels (e.g. 1000, 950, ... 4, 3, 2.2, 1.7, 1.3, 1 hPa), and then bin the data into 2-h local solar time (LST) bins in every 5° latitude band. Generally the COSMIC satellite configuration results in denser RO soundings in the mid-latitude and high latitude compared with tropics. For example, in the year 2007, the monthly average numbers of COSMIC soundings at a 2-h bin is about 54 in a 5°-latitude band centered at 5° N, 87 at

25° N, 125 at 50° N and 37 at 75° N, which equivalently correspond to the numbers per 500×500 km^2 per month: 8 at 5° N, 15 at 25° N, 26 at 50° N and 20 at 75° N. Roughly 75% RO soundings reach at 800 hPa ($\sim$2 km) and about 40% reach 950 hPa ($\sim$0.5 km) above MSL. However, due to topography over continental area, the exact percentage of RO soundings reaching the lowest 2 km above the Earth surface is actually higher. The zonal mean temperature T and refractivity N at the 12 local time bins are derived on a monthly basis. After the mean is removed, a harmonic analysis with 24-h and 12-h components is applied to compute the diurnal and semi-diurnal amplitudes and their phases for each latitude and height bin (Chapman and Lindzen, 1970; Wu et al., 1995; Dai et al., 2002). A brief summary of the harmonic analysis method is given below.

Given a time series y_i, $i = 1, 2, \cdots, M$, (M is the maximum number of samples for a day, in this study, $M = 12$) as a function of local solar time (LST) t_i, it can be decomposed into three components:

$$y_i(t_i) = \overline{y} + \sum_n S_n(t_i) + \varsigma \tag{3}$$

where, $\overline{y}$ is the daily mean; S_n is the harmonics with different periods and ς the residual noise. The harmonics with different time scales can be expressed as:

$$S_n(t_i) = A_n \cos(nt' - \phi) = a_n \cos(nt') + b_n \sin(nt') \tag{4}$$

where, t' is LST in 2π/day (i.e. $t' = 2\pi t_i / 24$ where t_i is LST in hours), $n = 1, 2, 3, 4,$ $\ldots$ denotes harmonics with periods of 24, 12, 8, 6, $\ldots$ hours, respectively; A_n is the amplitude (note that the peak-to-peak amplitude is $2A_n$); ϕ is the phase (time of the maximum y_i in LST). Here, we only focus on the two most dominant modes, i.e. the diurnal (S_1) and semi-diurnal (S_2) components.

Note that the observed time series could contain higher-order harmonics of the diurnal variations (such as period <12 h) and residuals (ς) due to measurement and sampling errors. The COSMIC sampling rate of local times might not be enough to catch those finer time scale (<12 h) variations. On the other hand, the zonal average

Atmospheric diurnal and semi-diurnal variations observed with GPS soundings

F. Xie et al.

Title Page

Abstract | Introduction

Conclusions | References

Tables | Figures

◄ | ►|

◄ | ►

Back | Close

Full Screen / Esc

Printer-friendly Version

Interactive Discussion

helps remove most of the longitudinal variability likely due to the planetary waves and nonmigrating tides (Wu et al., 1998) but the spectral aliasing from other wave components may induce additional error to the diurnal and semi-diurnal components of interest. The signal-to-noise ratio (SNR) of the derived amplitudes is thus calculated as the ratio of the remaining error after the diurnal and semi-diurnal fitting over the fitted amplitude (i.e. ς/A_n).

3 Tropical tidal waves

The migrating atmospheric tide in the tropical region, investigated for decades, is one of the most well-observed and understood phenomena among other tropical variabilities. It is a weak variation in terms of magnitude, and can be used as good validation on the RO sensitivity and the retrieval quality. In this section, we derive and characterize the vertical distribution of this tidal wave with the COSMIC RO measurements, and validate the results against some of the earlier studies.

3.1 Vertical structure of the migrating tides

To derive the vertical distribution of the propagating diurnal component, the tropical (10° S–10° N) COSMIC temperature and refractivity soundings in 2007 (a total of 361 051 profiles) are used. Figures 1 and 2 show, respectively, the vertical structure of diurnal and semi-diurnal amplitudes (left panels) and phases (i.e. the LST of the maximum amplitude, in right panels) for temperature (upper panels, in Kelvin) and refractivity (lower panels, in percentage) extracted from the monthly averaged data. Note that the total number of RO samples in 2008 (284 227 profiles) is about 20% less than in 2007 due to the lack of ground reference sites in the early 2008, however, very similar vertical structure of diurnal and semi-diurnal variations are derived based on the COSMIC 2008 soundings (not shown).

The propagating tidal wave, which migrates with the sun, dominates the tropical diurnal variation in the stratosphere and higher altitudes (e.g. McLandress, 1997). Its propagation nature is evident in the temperature and refractivity data, showing a downward progressing phase profile (Fig. 1b and d) with growing amplitude above 140 hPa (∼14 km). The vertical wavelength of the diurnal tidal wave is about 25 km, which is observed in both the temperature and refractivity phase profile. The migrating tidal wave observed by COSMIC is consistent with one obtained by Zeng et al. (2008) from the multiyear CHAMP data, the classical tidal theory and model results (e.g. Chapman and Linzen, 1970; McLandress, 1997). In the stratosphere the maximum refractivity amplitude reaches ∼1%, which corresponds to ∼2.5 K in temperature.

The refractivity and temperature fluctuations are related through Eq. (2) and through the hydrostatic balance equation embedded in the retrieval. Above ∼350 hPa (∼8 km), refractivity variations are dominated by temperature changes and their variations should be out of phase (e.g. 12 h difference) at constant pressure levels according to Eq. (2), which is consistent with the observed phase profiles. In addition, the amplitude profiles of the refractivity and temperature variations at these altitudes should be consistent in percentage as well, as seen in Fig. 1a and c, showing local minimums at 120 hPa (∼15 km) and 40 hPa (∼22 km) and a growing trend above 120 hPa (∼15 km). The minimum diurnal amplitude of temperature (∼0.1 K) and refractivity (∼0.05%) is found at 120 hPa (∼15 km). Local maximum diurnal amplitude in both temperature (0.9 K) and refractivity (∼0.4%) is found at around 9 hPa (∼32 km).

Above 40 km, although the temperature retrieval is not available, the refractivity data can be still used to derive atmospheric diurnal variations. Phase and amplitude structure shown in Fig. 1c and d are consistent with the expected upward propagating diurnal tidal mode despite the noisier phase structure and larger monthly variations in amplitude. At and above 140 hPa (∼14 km), the winter and autumn season shows larger diurnal amplitude compared to the summer and spring seasons. Between 350 hPa (∼8 km) and 260 hPa (∼10 km), spring season shows largest diurnal amplitude in temperature and refractivity. Below 5 km, again, the spring season exhibits the largest

ı◄ | ►ı

◄ | ►

Back | Close

Full Screen / Esc

diurnal amplitude in a year. As the diurnal tide propagates up to the upper stratosphere, the propagating wave component excited from tropospheric water vapor will interfere with the wave component excited by ozone heating, which can lead to larger variability in the migrating diurnal tide (Chapman and Lindzen, 1970). Note that the tidal wave amplitude tends to increase at higher altitude due to the exponential decay of the air density (Chapman and Linzen, 1970; McLandress, 1997). However, ozone heating becomes significant above 12 hPa (30 km) and reaches maximum around 1 hPa (47 km) (McLandress, 1997). The temperature variation due to ozone heating tends to reach maximum at local noon when maximum solar radiance is absorbed by ozone. The temperature tides is off phase compared with the fixed phase (12 noon) due to ozone heating, which could result in the change of the slope of the phase around 12 hPa (~30 km) and lead to non-monotonic structure of tidal amplitude at higher altitudes.

The diurnal variation below 90 hPa (~17 km) is complicated by the coexistence of wave forcings and propagation in the region. Figure 1b shows that at 260~140 hPa (or 10~14 km) the phase of the diurnal temperature variation remains rather constant (at ~6 p.m.), but shifts sharply at a few km above that. Similar behavior can be observed from the refractivity (Fig. 1d) but with the phase at 10~14 km relatively constant at 6 a.m. It is reflected in the slope of the diurnal phase, which changes at 90 hPa (~17 km) and remains relatively constant up to 40 km. In the PBL, the diurnal variation can be large (0.35% at 800 hPa) as well, which is equivalent to ~1 K in temperature (if solely caused by temperature variation) or ~2.5% in specific humidity.

Due to the non-sinusoidal shape of diurnal solar forcing along with various feedback mechanisms, the daily oscillation cannot be fully represented by a sinusoidal cycle. As discussed in Eq. (2) in Sect. 3.2, the secondary sub-daily variation, i.e. the semi-diurnal variation can also be resolved given 12 LST observations. Figure 2 shows that the amplitude is generally weaker but comparable to the diurnal one in the lower troposphere. The amplitude decreases with altitude and reaches the minimum (about 0.1%) at around 10 km and then slightly increases amplitude throughout the stratosphere with the maximum reaching roughly 0.5% in refractivity (~1.3 K) at 1 hPa (~47 km).

Contrary to the rather organized diurnal phase structure, the semi-diurnal temperature and refractivity phases are rather irregular at all altitudes.

The semidiurnal amplitude also shows large month-to-month variability, and can be slightly larger than the diurnal one in the troposphere and in spring season above 12 hPa (∼30 km). It is interesting to note that this happens mostly below 400 hPa (∼7 km) but less frequently above this level (i.e. in the stratosphere), where migrating diurnal tide dominates intradaily variations. At the PBL levels, the semidiurnal amplitude also has relatively large magnitude close to 0.45% in refractivity at 800 hPa (∼2 km), slightly larger than the diurnal one.

4 Seasonal variations

The seasonal variation of the migrating component of tidal waves can be clearly seen at all pressures in the stratosphere, and Fig. 3 illustrates this with the two year (2007–2008) time series at 30 hPa. The maximum amplitude of the propagating diurnal temperature tide swings around the equator, depending on time of the year. During the northern-hemispheric winter and spring (November to March), the maximum diurnal temperature amplitude (∼1 K) occurs at around 5° N, whereas the maximum shifts to 5° S during the summer and autumn (June to September), which is opposite to where the solar forcing peaks. The similar seasonal variation was observed with UARS Microwave Limb Sounder data (Wu et al., 1998), CHAMP RO and in the 3-D Canadian Middle Atmosphere Model (CMAM) simulations (Zeng et al., 2008), but not in the simulations with Global-Scale Wave Model Version 2 (GSWM02) (Hagan and Forbes, 2002). The asymmetric structure of the propagating diurnal tide is more pronounced in the upper atmosphere, and more in the solstice months than in the equinox months (McLandress, 1997, 2002).

To characterize the seasonal variation of the diurnal amplitude at a broader altitude and latitude range, we analyze the global refractivity data at pressures from the

ACPD

9, 25409–25441, 2009

Atmospheric diurnal and semi-diurnal variations observed with GPS soundings

F. Xie et al.

Title Page

Abstract | Introduction

Conclusions | References

Tables | Figures

◄ | ►

◄ | ►

Back | Close

Full Screen / Esc

Printer-friendly Version

Interactive Discussion

surface to ~1 hPa. Figure 4 shows the results only at eight pressure levels. Above ~8 km, the refractivity variability mostly reflects temperature variations at the associated pressure level. Although the seasonal variation is similar between 2007 and 2008, interannual differences are evident in the monthly COSMIC data. For example, the amplitude at 12~1.3 hPa (30~45 km) and at 30° S–90° S has two maximums, occurring in February–April and September–October. The September-October maximum has larger amplitudes in 2007 than 2008, but it reverses for the February–April maximum that is located more toward the pole. At 30° N–90° N it shows only one maximum in February, which appears to be larger in amplitude in 2008. These high-latitude amplitudes (0.8–2%) are much greater than the tropical variability.

The 100 hPa level is where the tropical diurnal tide starts to propagate but its amplitude is too small to observe. The significant diurnal amplitudes at this level are mostly associated with vertically trapped components. It is interesting that February–March have the largest amplitude, showing maximums at 20° S, 30° N, and high latitudes for both 2007 and 2008. The subtropical maximums reduce substantially at 40 hPa, as a manifestation of vertically trapped modes. The underlying physical process for the seasonal variation of the diurnal amplitude at 100 hPa is unclear and requires further investigations involving numerical models.

At 40 hPa (~22 km), where the tropical tidal wave propagates freely, the tidal amplitude (~0.2%) becomes slightly larger compared to those at 260 hPa (~10 km) and 100 hPa (~16 km). Polar regions show generally larger seasonal variations than the tropics. For example, a maximum of over 1.8% refractivity variation (or ~3.6 K in temperature) is seen around February of both years at 80° N. While the maximum near the south pole is found in both April (0.8%) and October (1.2%) at 75° S. The maximum in October is larger in 2007 than in 2008.

At 12 hPa (~30 km), the diurnal amplitude maximum drifts around the equator between 5° S and 5° N, anti-correlated with the solar heating change, which peaks at the summertime subtropical latitude. The refractivity variation here is consistent with the diurnal temperature amplitude as seen in Fig. 3. Such seasonal variation in the 24-h

Atmospheric diurnal and semi-diurnal variations observed with GPS soundings

F. Xie et al.

Full Screen / Esc

Printer-friendly Version

Interactive Discussion

amplitude was also found in the study for the stratospheric tide by Zeng et al. (2008) and for the mesospheric tide by McLandress (1997, 2002). Again, polar regions show slightly larger diurnal amplitude than the tropics. The Arctic region shows only one maximum in seasonal variations of the diurnal refractivity amplitude (>1.4% or 3.5 K in temperature) in January–March. Double maximums are observed in Antarctic region with a weaker amplitude (0.8% or 2 K) in February–April, and a stronger one (1.4% or 3.5 K) during August–October at 70° S.

At 3 hPa (~40 km), the maximum diurnal amplitude in the tropics is almost doubled compared with that at 40 hPa (22 km). The peak diurnal amplitude in the Arctic reaches a value of >2%, while the double peaks in the Antarctic also increase to >1.2% (3 K) during February–April and over 2% (5 K) during August–October. The diurnal amplitude at 1.3 hPa (~45 km) shows rather similar pattern as 3 hPa (~40 km) but has slightly larger amplitude. The seasonal variation of the tropical diurnal tide becomes less asymmetric about the equator, compared to that in the lower altitudes. However, the seasonal patterns remain similar in both polar regions.

The diurnal amplitude of the refractivity is generally small (<1%) at 500–100 hPa (5.5~16 km) but becomes larger at altitudes below 500 hPa (~5.5 km). The 24-h amplitudes at 260 hPa show a distinct seasonal variation in the subtropics, which is similar to that at 100 hPa. Maximum diurnal amplitudes centered at 20° S and 30° N in February–March are observed at both altitudes, but the 260 hPa has slightly weaker amplitudes. At 500 hPa (~5.5 km) the 24-h amplitude begins to show significant influences of tropical water vapor in the lower troposphere, and the zonally-averaged amplitude is generally <1%. The maximums at high latitudes appear to occur roughly in the same periods when they are found at 260 and 100 hPa. The tropical diurnal amplitude shows a minimum in July–August, and a maximum in February–March.

At 800 hPa (~2 km), the zonal mean 24-h amplitude can be as high as 1% in refractivity, with subtropical seasonal minimums and maximums reversed from those seen at 500 hPa. The subtropics and the Antarctic show a maximum during the boreal summer months. Two peaks, centered at of 20° N (August~October) and 15° S (in October), are

observed in both years. The March maximum of the diurnal amplitude in the Antarctic is stronger in 2008 than in 2007.

The results at pressures over 800 hPa (<2 km) are not studied here because a frequent negative bias has been observed in the refractivity retrievals, likely contaminated by the presence of super-refraction or the ducting condition near the PBL top (Sokolovskiy, 2003; Xie et al., 2006; Ao, 2007). The biased RO retrievals are usually found in the tropical and subtropical PBL regions and need to be dealt with carefully (e.g. Xie et al., 2006). We will present the analysis near the PBL in a separate study.

5 Monthly climatology

In this section we analyze the vertical structures of diurnal and semi-diurnal refractivity amplitude as a function of latitude for four nominal months in 2007 (Fig. 5). Generally speaking, the diurnal and semi-diurnal amplitudes show relatively large values in the lower troposphere (>500 hPa) at low latitudes, and then decrease with height to a minimum value (∼0.2%) in the middle and upper troposphere before increasing above the tropopause. In the tropics and subtropics, double maximums can be seen for both hemispheres for all seasons in the lower troposphere, with relatively larger amplitude in the northern hemisphere. The positions of the maximums are asymmetric around equator and vary with season or the solar zenith angle, moving slightly to south in January and north in July.

The diurnal variation has significant amplitudes at low and high latitudes in the lower troposphere and stratosphere with strong seasonal variations. The tropical maximum in the stratosphere, as discussed above, is associated with the propagating diurnal tide. The vertical structure of the tide is asymmetric along the equator and tilted toward the summer hemisphere in January and July with a maximum at ∼10 hPa. The asymmetry is less prominent in April and October. It is interesting to observe that in April two maximums are located at ∼100 hPa in the subtropics, showing a relatively large diurnal amplitude (∼0.4% at 30° N and ∼0.2% at 30° S).

Title Page

Abstract | Introduction

Conclusions | References

Tables | Figures

◄ | ►

◄ | ►

Back | Close

Full Screen / Esc

Printer-friendly Version

Interactive Discussion

In stratosphere, the diurnal amplitude is generally greater at high latitudes than those at the low latitudes for all seasons. There are two maximums at $\sim$80° N ($\sim$80° S) in January (October), peaking at $\sim$30 and 2 hPa, but the double maximum structure is not very clear in July. The wintertime Arctic maximums reach a value over 1.6% in January, approximately four times greater than the July background amplitude in the Antarctic stratosphere during the austral winter, and twice as large as the springtime Antarctic amplitude in October. In January, a maximum is confined within a narrow layer in the Antarctic, centered at 200 hPa ($\sim$12 km) with amplitude about 0.4% ($\sim$1 K). This trapped diurnal feature is characterized by a minimum at 50 hPa ($\sim$20 km) before further growing with height above that. This summertime polar feature is not so pronounced in July of north pole, but the growing nature in the upper stratosphere is similar. Compared to January, the polar wintertime amplitude in July is shifted slightly to mid-latitudes where cloud bands and diurnal solar forcing are present. During these months the region 80° poleward in the winter hemisphere has no sunlight, and therefore the observed diurnal variations must result from indirect effects in atmospheric dynamics.

The semidiurnal amplitude exhibits a vertical distribution similar to the diurnal one, showing high values in the lower troposphere with double subtropical maximums for the four months. In January and October the double vertical maximums in the polar region are also consistent with the patterns seen with the diurnal amplitude. One of the reasons for the consistent diurnal and semidiurnal amplitude distribution is that atmospheric diurnal variations are not sinusoidal. When a non-sinusoidal variation is fitted with the 12-h and 24-h sinusoidal functions, both components can respond with large amplitude. Weak in the tropics, the semidiurnal tide excited from tropospheric water vapor heating is not supported to propagate vertically at low latitudes.

6 Discussion

The two-year COSMIC RO observations provide valuable information on the global diurnal and semi-diurnal variations with high vertical resolution, which has important implications for weather and climate research. The seasonal variation and vertical distribution of the observed diurnal cycle in the troposphere and stratosphere are not well understood, although tropical diurnal tide has been studied and documented intensively in the past.

The tropical diurnal tidal wave, despite weak in amplitude, is well observed by the high resolution GPS RO technique. Consistent with the CMAM model simulation, the vertical profiles of the tidal amplitude and phase derived from the COSMIC data serve as a validation source for the RO observations. Above the dry upper troposphere (∼8 km in tropics), the diurnal temperature and refractivity variations are out of phase, as expected for the upward propagating tidal wave above 140 hPa (∼14 km). The region between 350 hPa and 100 hPa is dominated by the water vapor solar heating, which possibly explains the locked diurnal phase in temperature (e.g. 18:00 LST in Fig. 1b). The solar heating in the tropics tends to peak in the late afternoon, large part of which is driven by the heating over land.

The diurnal variation in the data-sparse polar region, however, is much less known and poorly understood. The sampling with COMSIC RO is the best data source at present to study the diurnal cycle in this region since the regular once-daily or twice-daily radiosonde measurements cannot resolve the diurnal cycle. Radar and lidar measurements are sparse and limited mostly in the mesosphere and lower thermosphere. In this study we found not only significant diurnal and semidiurnal amplitudes in the polar region but also substantial differences between the Arctic and the Antarctic. The diurnal amplitude in the Antarctic (around 75° S) prevails through all seasons but the maximum amplitude occurs at different altitudes. In contrast, the Arctic diurnal amplitude maximizes in the boreal winter and spring. All these diurnal features are statistically significant, showing SNR>3. The underlying physical mechanism(s) for the polar

diurnal variability is unclear, especially during polar nights when the solar heating is absent.

Although the COSMIC six satellites were spread out far enough for diurnal sampling in 2007, in the polar region, the local time sampling is still not uniform compared with year 2008. The consistent pattern of diurnal and semi-diurnal amplitude derived from both years indicates the un-even sampling should not contribute significantly to the diurnal sampling errors. On the other hand, the relatively low samples at polar region (e.g. ~37 at 75° S or 75° N in a monthly mean, 2-h, 5°-latitude bin during 2007) may not be sufficient to average out contributions from planetary waves. Thus, spectral leakage from insufficient sampling could induce non-negligible aliasing error. To verify robustness of the derived RO diurnal amplitudes, we further analyzed the COSMIC RO measurements in 2007 and 2008 provided by UCAR (University Corporation for Atmospheric Research). The UCAR single differencing (Wickert et al., 2002) technique yields ~40% more RO profiles in 2007 and ~55% more in 2008, globally, compared to the JPL algorithm that applies the double differencing technique. In the polar region, the RO samples from UCAR are twice more than ones from JPL but the structure of diurnal and semi-diurnal amplitude remains largely unchanged below 12 hPa (~30 km) for both 2007 and 2008 (not shown). Both the diurnal and semi-diurnal amplitude are generally reduced by less than 20% overall. However, the diurnal amplitude is reduced by about 40% over north polar stratosphere between 100 hPa and 30 hPa around 75° N in January 2007. Another similar reduction of diurnal amplitude is found in south polar stratosphere at around 80° S in April 2008. This suggests that to first order the diurnal/semidiurnal amplitude extracted from the GPSRO (JPL retrieval) is statistically significant and the aliasing from under-sampling is non-negligible in some months but plays a secondary role overall. Quantitatively evaluation of the aliasing errors due to the un-even and insufficient sampling would require further spectrum analysis (e.g. Wu et al., 1995).

Above 12 hPa, however, the UCAR retrievals show significantly smaller amplitude compared to the JPL retrieval at all latitudes. In addition, the zonal mean variance

Atmospheric diurnal and semi-diurnal variations observed with GPS soundings

F. Xie et al.

of UCAR temperature and refractivity retrievals shows almost the same magnitudes to JPL retrievals at altitudes below 12 hPa but significantly smaller values above that level. This is likely due to different upper boundary treatments implemented in the UCAR and JPL retrievals (Ho et al., 2009). For example, in JPL retrieval, no climatology information is used whereas the UCAR retrieval uses a complicated dynamic optimization method that combines a priori (least square fit of raw bending angle) and observed bending angles. Such a constraint to a priori can help to stabilize the retrievals in the very noise case but could also cause less variability.

In the lower troposphere the phase of the refractivity diurnal variation shows large month-to-month variability in the tropics (Fig. 1d), not locked to a specific local time, because of complex processes near the surface. Not only in the tropics but also at middle and high latitudes, the refractivity in the lower troposphere is strongly influenced by water vapor abundance and driven by the hydrological and dynamical processes near the surface. Studying three-hourly weather data from 15 000 worldwide stations, Dai (2001) found that the most frequent (morning) hour of showery precipitation over water is out of phase with those over land and the latter exhibited large seasonal variability. Similar large variability was also reported in wind measurements (Dai and Deser, 1999) and cloud and water vapor data (Soden, 2000; Tian et al., 2004).

To improve the measurements in the PBL, the GPS RO technique needs (1) to enhance its ability of receiving transmitter signal in the presence of large PBL water vapor variability, and (2) to better understand and remove the negative refractivity bias often found in the bottom of each occultation profile. The COSMIC RO constellation have greatly improved (1) with the open-loop receivers and significantly increased the percentage of the RO observations inside the PBL (i.e. the lowest 2~3 km atmosphere above the earth surface). However, investigations of the PBL are beyond the scope of this paper, and the problem of frequent negative biases in the refractivity retrieval remain to be corrected, which is likely caused by the super-refraction or the ducting near the PBL top (Sokolovskiy, 2003; Xie et al., 2006; Ao, 2007). One of the advantages with global high-resolution bias-free RO measurements is to be able to resolve

the PBL. A 100 m vertical resolution is achievable as the technology improves, and a better understanding of the PBL dynamics has important implications for climate and weather research.

Finally, the RO signals are sensitive to ionospheric structure and perturbations. Ionospheric residuals may affect the diurnal variation observed in the neutral atmospheric parameters (e.g. bending and refractivity), especially in the cases of weak atmospheric signals. Although an ionospheric correction has been made through a linear combination of L1 and L2 bending angle retrievals at a given impact parameter (Vorob'ev and Krasil'nikova, 1994), higher-order residual errors could remain (e.g. Syndergaard, 2000). The ionospheric residual errors could have diurnal variations related to ionospheric electron density and affect the signal derived in the upper stratosphere.

The observed diurnal variations have an important implication for monitoring the global warming trend in the future. Valuable for establishing a consistent, long-term observation, the GPS RO technique is based on the fundament SI unit in atomic clock calibration and insensitive to orbit geometry and clouds (Schrøder et al., 2003). However, like other climate observing systems, the sampling must be adequately uniform without biased to certain local times nor to specific geographical locations since climate change signals may be so subtle that any of these biases can be misinterpreted. As shown in Fig. 1c, over the tropics the annual zonal mean of diurnal amplitude is roughly 0.4% in refractivity or roughly 1 K in temperature at 800 hPa (~2 km) altitude; and reaches up to 1% in refractivity (or 2.5 K) at 1 hPa (~47 km) altitude. Polar regions show even larger diurnal amplitude in the stratosphere with strong seasonal variability. Such complicated vertical and spatial diurnal variation pattern needs to be carefully evaluated and adequately understood in studying climate changes.

7 Conclusion and future work

In this paper, we derived the latitudinal and vertical distributions of the diurnal and semidiurnal variations in temperature and refractivity using two-year COSMIC RO

soundings. The tropical zonally-averaged diurnal amplitude and phase clearly show the migrating tidal waves, which propagate upwards from around 140 hPa (∼14 km) to the upper stratosphere (Fig. 1). The annual mean diurnal amplitude shows a local maximum of about 0.4% in refractivity (or 1 K in temperature) close to the PBL top (800 hPa or 2 km) and decreases to a minimum of 0.05% (or 0.1 K) at 140 hPa (∼14 km); then increases to a maximum of 1% (or 2.5 K) at 1 hPa (∼47 km) in the stratosphere. At and below 500 hPa (∼5.5 km), the seasonal variation of the maximum diurnal amplitude generally follows the apparent motion of the sun. However, at 30 km the maximum 24-h amplitude is out of the phase of the solar heating (Fig. 4).

The vertical structure of zonal mean diurnal variations shows rather similar pattern and comparable magnitude to the semi-diurnal variations (Fig. 5). The lower troposphere (below 500 hPa) shows relatively large diurnal and semi-diurnal amplitude in the tropics and mid-latitude regions. The location of the peak diurnal amplitude of lower troposphere follows the solar heating in the tropics. Overall, the diurnal amplitude increases with decreasing height in the lower troposphere. The minimum of the 24-h refractivity amplitude is found near the tropopause height and increases again at higher altitudes. Moreover, south polar region shows a large diurnal amplitude in the stratosphere throughout the year. While in the north polar region, only in January and April, large diurnal amplitude (statistical significant) is found to dip into the lower stratosphere.

Further studies are needed to understand causes and consequences of the diurnal variations in the polar stratosphere. It would be also very interesting to look into the diurnal variations inside the PBL, where differential heating due to land and ocean contrast becomes important. However, the limited sounding samples for the current COSMIC observations and the negative bias in the RO refractivity measurements in the tropical and subtropical regions would need to be carefully considered before applying for diurnal analysis.

The diurnal variations observed by COSMIC RO soundings have important implication for detecting and monitoring climate changes in the future satellite missions.

Insufficient diurnal sampling in climate trend monitoring could lead to biases in the detected climate trend. Future RO missions, such as the 12-satellite COSMIC-II concept, will double the sampling density of the current COSMIC observations. Such a dense sounding will enable more accurate determination of the diurnal variation on a global as well as regional basis.

References

Anthes, R. A., Bernhardt, P. A., Chen, Y., et al.: The COSMIC/FORMOSAT-3 mission early results, B. Am. Meteorol. Soc., 89(1), 313–333, doi:10.1175/BAMS-89-3-313, 2008.

Ao, C. O., Meehan, T. K., Hajj, G. A., Mannucci, A. J., and Beyerle, G.: Lower-troposphere refractivity bias in GPS occultation retrievals, J. Geophys. Res., 108(D18), 4577, doi:10.1029/2002JD003216, 2003.

Ao, C. O.: Effect of ducting on radio occultation measurements: An assessment based on high-resolution radiosonde soundings, Radio Sci., 42, RS2008, doi:10.1029/2006RS003485, 2007.

Ao, C. O., Hajj, G. A., Meehan, T. K., Dong, D., Iijima, B. A., Mannucci, A. J., and Kursinski, E. R.: Rising and setting GPS occultations by use of open-loop tracking, J. Geophys. Res., 114, D04101, doi:10.1029/2008JD010483, 2009.

Betts, A. K. and Jakob, C.: Evaluation of the diurnal cycle of precipitation, surface thermo-dynamics, and surface fluxes in the ECMWF model using LBA data, J. Geophys. Res., 107(D20), 8045, doi:10.1029/ 2001JD000427, 2002.

Beyerle, G., Gorbunov, M., and Ao, C. O.: Simulation studies of GPS radio occultation measurements, Radio Sci., 38(5), 1084, doi:10.1029/2002RS002800, 2003.

Atmospheric diurnal and semi-diurnal variations observed with GPS soundings

F. Xie et al.

Chapman, S. and Lindzen, R. S.: Atmospheric Tides Thermal and Gravitational, D. Reidel, Dordrecht, Holland, 200 pp., 1970.

Chung, E. S., Sohn, B. J., Schmetz, J., and Koenig, M.: Diurnal variation of upper tropospheric humidity and its relations to convective activities over tropical Africa, Atmos. Chem. Phys., 7, 2489–2502, 2007,
http://www.atmos-chem-phys.net/7/2489/2007/.

Dai, A.: Recent Changes in the Diurnal Cycle of Precipitation Over the United States, Geophys. Res. Lett., 26(1), 341–344, 1999.

Dai, A. and Deser, C.: Diurnal and semidiurnal variations in global surface wind and divergence fields, J. Geophys. Res., 104(D24), 31109–31125, 1999.

Dai, A., Giorgi, F., and Trenberth, K.: Observed and model-simulated diurnal cycles of precipitation over the contiguous United States, J. Geophys. Res., 104(D6), 6377–6402, 1999.

Dai, A.: Global precipitation and thunderstorm frequencies, Part II: Diurnal variations, J. Climate, 14, 1112–1128, 2001.

Dai, A. and Trenberth, K. E.: The diurnal cycle and its depiction in the Community Climate System Model, J. Climate, 17, 930–951, 2004.

Dai, A., Wang, J. H., Ware, R. H., and Hove, T. V.: Diurnal variation in water vapor over North America and its implications for sampling errors in radiosonde humidity, J. Geophys. Res, 107(D10), 4090, doi:10.1029/2001JD000642, 2002.

Hagan, M. E. and Forbes, J. M.: Migrating and nonmigrating diurnal tides in the middle and upper atmosphere excited by tropospheric latent heat release, J. Geophys. Res., 107(D24), 4754, doi:10.1029/2001JD001236, 2002.

Hajj, G. A., Kursinski, E. R., Romans, L. J., Bertiger, W. I., and Leroy, S. S.: A technical description of atmospheric sounding by GPS occultation, J. Atmos. Sol.-Terr. Phy., 64(2), 451–469, 2002.

Hays, P. B., Wu, D. L., and HRDI Science Team: Observations of the diurnal tide from space, J. Atmos. Sci., 51(20), 3077–3093, 1994.

Healy, S. B. and Eyre, J. R.: Retrieving temperature, water vapour and surface pressure information from refractive index profiles derived by radio occultation: a simulation study, Q. J. Roy. Meteorol. Soc., 126, 1661–1683, 2000.

Ho, S.-P., Kirchengast, G., Leroy, S., et al.: Estimating the Uncertainty of using GPS Radio Occultation Data for Climate Monitoring: Inter-comparison of CHAMP Refractivity Climate Records 2002–2006 from Different Data Centers, J. Geophys. Res., in press, 2009.

Atmospheric diurnal and semi-diurnal variations observed with GPS soundings

F. Xie et al.

Title Page

Abstract	Introduction
Conclusions	References
Tables	Figures

|◄ | ►|

◄ | ►

Back | Close

Full Screen / Esc

Printer-friendly Version

Interactive Discussion

Huang, C. M., Zhang, S. D., and Yi, F.: Intensive radiosonde observations of the diurnal tide and planetary waves in the lower atmosphere over Yichang (111°18′ E, 30°42′ N), China, Ann. Geophys., 27, 1079–1095, 2009, http://www.ann-geophys.net/27/1079/2009/.

Keckhut, P., Wild, J. D., Gelman, M., Miller, A. J., and Hauchecorne, A.: Investigations on long-term temperature changes in the upper stratosphere using lidar data and NCEP analyses, J. Geophys. Res., 106(D8), 7937–7944, 2001.

Kuo, Y. H., Wee, T. K., Sokolovskiy, S., Rocken, C., Schreiner, W., Hunt, D., and Anthes, R. A.: Inversion and error estimation of GPS radio occultation data, J. Meteorol. Soc. Jpn., 82(1B), 507–531, 2004.

Kursinski, E. R., Hajj, G. A., Schofield, J. T., Linfield, R. P., and Hardy, K. R.: Observing Earth's atmosphere with radio occultation measurements using the Global Positioning System, J. Geophys. Res., 102, 23429–23465, 1997.

Kursinski, E. R., Healy, S. B., and Romans, L. J.: Initial results of combining GPS occultations with ECMWF global analyses within a 1DVar framework, Earth Planets Space, 52, 885–892, 2000.

Lieberman, R. S. and Leovy, C. B.: A numerical model of nonmigrating diurnal tides between the surface and 65 km, J. Atmos. Sci., 52, 389–409, 1995.

Lieberman, R. S., Ortland, D. A., and Yarosh, E. S.: Climatology and interannual variability of diurnal water vapor heating, J. Geophys. Res., 108(D3), 4123, doi:10.1029/2002JD002308, 2003.

Lin, X., Randall, D. A., and Fowler, L. D.: Diurnal variability of the hydrologic cycle and radiative fluxes: Comparisons between observations and a GCM, J. Climate, 13, 4159–4179, 2000.

McLandress, C., Shepherd, G. G., and Solheim, B. H.: Satellite observations of thermospheric tides: Results from the Wind Imaging Interferometer on UARS, J. Geophys. Res., 101(D2), 4093–4114, 1996.

McLandress, C.: Seasonal variability of the diurnal tide: Results from the Canadian Middle atmospheric general circulation model, J. Geophys. Res., 102, 29747–29764, 1997.

McLandress, C.: The Seasonal Variation of the Propagating Diurnal Tide in the Mesosphere and Lower Thermosphere, Part II: The Role of Tidal Heating and Zonal Mean Winds, J. Atmos. Sci., 59(5), 907–922, 2002.

Neale, R. and Slingo, J.: The maritime continent and its role in the global climate: A GCM study, J. Climate, 16, 834–848, 2003.

Atmospheric diurnal and semi-diurnal variations observed with GPS soundings

F. Xie et al.

Title Page

Abstract	Introduction
Conclusions	References
Tables	Figures

|◄ | ►|

◄ | ►

Back | Close

Full Screen / Esc

Printer-friendly Version

Interactive Discussion

Nesbitt, S. W. and Zipser, E. J.: The diurnal cycle of rainfall and convective intensity according to three years of TRMM measurements, J. Climate, 16, 1456–1475, 2003.

Poli, P., Joiner, J., and Kursinski, E. R.: 1DVAR analysis of temperature and humidity using GPS radio occultation refractivity data, J. Geophys. Res., 107, D20448, doi:10.1029/2001JD000935, 2002.

Pirscher, B., Foelsche, U., Lackner, B. C., and Kirchengast, G.: Local time influence in single-satellite radio occultation climatologies from Sun-synchronous and non-Sun-synchronous satellites, J. Geophys. Res., 112, D11119, doi:10.1029/2006JD007934, 2007.

Randall, D. A., Harshvardhan, and Dazlich, D. A.: Diurnal variability of the hydrologic cycle in a general circulation model, J. Atmos. Sci., 48, 40–62, 1991.

Rocken, C., Anthes, R., Exner, M., et al.: Analysis and validation of GPS/MET data in the neutral atmosphere, J. Geophys. Res., 102, 29849–29866, 1997.

Schreiner, W., Rocken, C., Sokolovskiy, S., Syndergaard, S., and Hunt, D.: Estimates of the precision of GPS radio occultations from the COSMIC/FORMOSAT-3 mission, Geophys. Res. Lett., 34, L04808, doi:10.1029/2006GL027557, 2007.

Schröder, T., Leroy, S., Stendel, M., and Kaas, E.: Validating the microwave sounding unit stratospheric record using GPS occultation, Geophys. Res. Lett., 30(14), 1734, doi:10.1029/2003GL017588, 2003.

She, C. Y., Chen, S., Williams, B. P., Hu, Z., Krueger, D. A., and Hagan, M. E.: Tides in the mesopause region over Fort Collins, Colorado (41° N, 105° W) based on lidar temperature observations covering full diurnal cycles, J. Geophys. Res., 107(D18), 4350, doi:10.1029/2001JD001189, 2002.

Slingo, A., Wilderspin, R. C., and Brentnall, S. J.: Simulations of the diurnal cycle of outgoing longwave radiation with an atmospheric GCM, Mon. Weather Rev., 115, 1451–1457, 1987.

Smith, E. K. and Weintraub, S.: The constants in the equation for atmospheric refractive index at radio frequencies, Proc. IRE, 41, 1035–1037, 1953.

Soden, B. J., Tjemkes, S., Schmetz, J., et al.: An intercomparison of radiation codes for retrieving upper tropospheric water vapor in the 6.3 mm band, B. Am. Meteorol. Soc., 81, 797–808, 2000.

Sokolovskiy, S. V.: Effect of superrefraction on inversions of radio occultation signals in the lower troposphere, Radio Sci., 38, 1058, doi:10.1029/2002RS002728, 2003.

Sokolovskiy, S., Kuo, Y.-H., Rocken, C., Schreiner, W. S., Hunt, D., and Anthes, R. A.: Monitoring the atmospheric boundary layer by GPS radio occultation signals recorded in the

open-loop mode, Geophys. Res. Lett., 33, L12813, doi:10.1029/2006GL025955, 2006.

States, R. J. and Gardner, C. S.: Temperature structure of the mesopause region (80–105 km) at 40° N latitude, 2, Diurnal variations, J. Atmos. Sci., 57, 78–92, 2000.

Syndergaard, S.: On the ionosphere calibration in GPS radio occultation measurements, Radio Sci., 35, 865–883, 2000.

Tian, B., Soden, B. J., and Wu, X.: Diurnal cycle of convection, clouds, and water vapor in the tropical upper troposphere: Satellites versus a general circulation model, J. Geophys. Res., 109, D10101, doi:10.1029/2003JD004117, 2004.

Tian, B., Held, I. M., Lau, N.-C., and Soden, B. J.: Diurnal cycle of summertime deep convection over North America: A satellite perspective, J. Geophys. Res., 110, D08108, doi:10.1029/2004JD005275, 2005.

Tsuda, T., Kato, S., Manson, A. H., and Meek, C. E.: Characteristics of semidiurnal tides observed by the Kyoto meteor radar and Saskatoon medium-frequency radar, J. Geophys. Res., 93, 7027–7036, 1988.

Tsuda, T., Murayama, Y., Wiryosumarto, H., Harijono, S. W. B., and Kato, S.: Radiosonde observations of equatorial atmosphere dynamics over Indonesia, 1. Equatorial waves and diurnal tides, J. Geophys. Res., 99(D5), 10491–10505, 1994.

Vorobev, V. V. and Krasil'nikova, T. G.: Estimation of the accuracy of the atmospheric refractive index recovery from Doppler shift measurements at frequencies used in the NAVSTAR system, Physics of the Atmosphere and Ocean, 29(5), 602–609, 1994.

Wickert, J., Beyerle, G., Hajj, G. A., Schwieger, V., and Reigber, C.: GPS radio occultation with CHAMP: Atmospheric profiling utilizing the space-based single difference technique, Geophys. Res. Lett., 29(8), 1187, doi:10.1029/2001GL013982, 2002.

Williams, B. P., She, C. Y., and Roble, R. G.: Seasonal climatology of the nighttime tidal perturbation of temperature in the midlatitude mesopause region, Geophys. Res. Lett., 25, 3301–3304, 1998.

Wu, D. L., Hays, P. B., and Skinner, W. R.: A least squares method for spectral analysis of space-time series, J. Atmos. Sci., 52(20), 3501–3511, 1995.

Wu, D. L., McLandress, C., Read, W. G., Waters, J. W., and Froidevaux, L.: Equatorial diurnal variations observed in UARS Microwave Limb Sounder temperature during 1991–1994 and simulated by the Canadian Middle Atmosphere Model, J. Geophys. Res., 103(D8), 8909–8917, 1998.

Xie, F., Syndergaard, S., Kursinski, E. R., and Herman, B. M.: An Approach for Retrieving

Atmospheric diurnal and semi-diurnal variations observed with GPS soundings

F. Xie et al.

Marine Boundary Layer Refractivity from GPS Occultation Data in the Presence of Super-refraction, J. Atmos. Ocean. Tech., 23, 1629–1644, 2006.

Xie, F., Haase, J. S., and Syndergaard, S.: Profiling the Atmosphere Using the Airborne GPS Radio Occultation Technique: A Sensitivity Study, IEEE T. Geosci. Remote, 46(11), 3424–3435, doi:10.1109/TGRS.2008.2004713, 2008.

Yang, G.-Y. and Slingo, J. M.: The diurnal cycle in the tropics, Mon. Weather Rev., 129, 784–801, 2001.

Zeng, Z., Randel, W., Sokolovskiy, S., Deser, C., Kuo, Y.-H., Hagan, M., Du, J., and Ward, W.: Detection of migrating diurnal tide in the tropical upper troposphere and lower stratosphere using the Challenging Minisatellite Payload radio occultation data, J. Geophys. Res., 113, D03102, doi:10.1029/2007JD008725, 2008.

Atmospheric diurnal and semi-diurnal variations observed with GPS soundings

F. Xie et al.

Title Page

Abstract | Introduction

Conclusions | References

Tables | Figures

◄ | ►

◄ | ►

Back | Close

Full Screen / Esc

Printer-friendly Version

Interactive Discussion
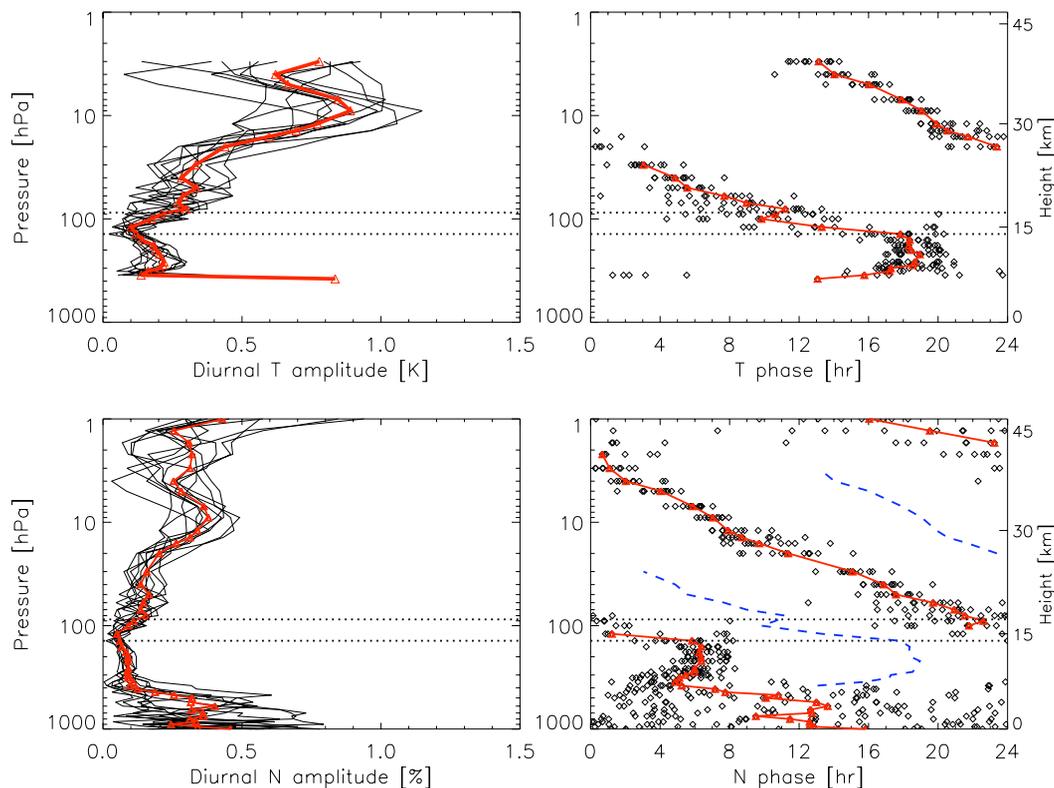
Fig. 1. Vertical structure of the temperature (upper panels) and refractivity (lower panels) amplitude (left panels) and phase (right panels) of diurnal variations over 10° S~10° N based on COSMIC RO observations in 2007. Black lines (left panels) represent 12 monthly mean amplitude profiles whereas phases from the monthly data are shown as open diamond (right panels). The RED thick lines show the annual median values. The blue dashed lines in the lower right panel represents the temperature phase as shown in the upper right panel.
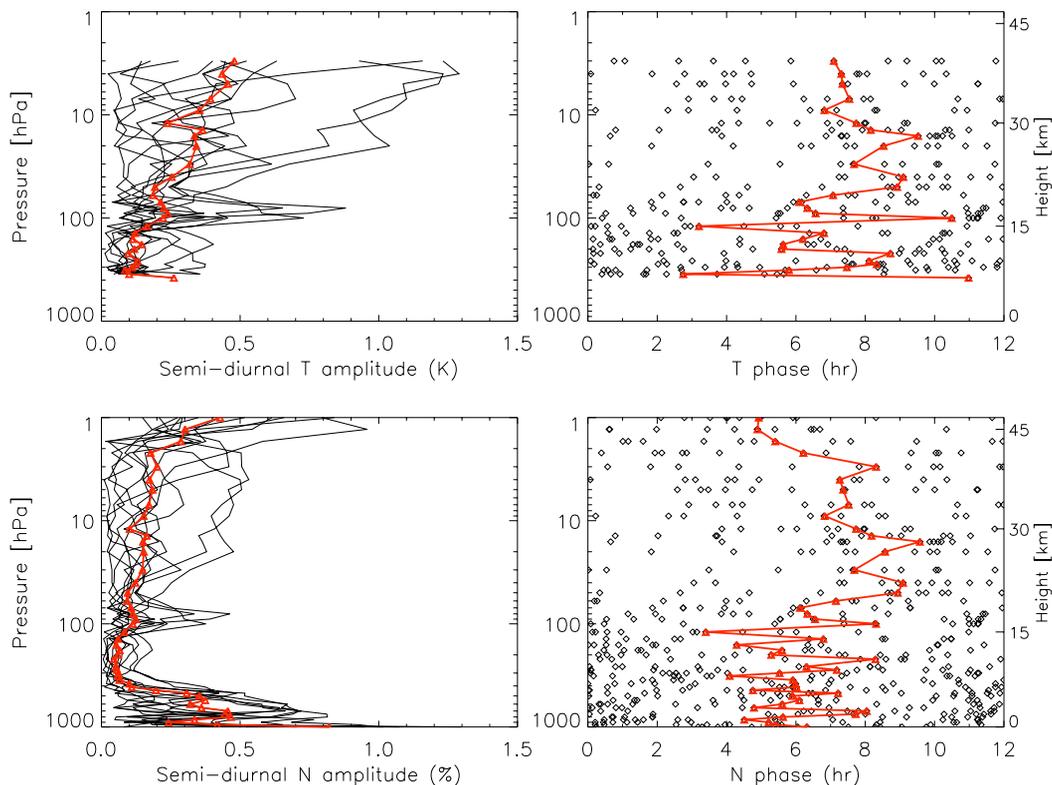
Fig. 2. Vertical structure of the temperature (upper panels) and refractivity (lower panels) amplitude (left panels) and phase (right panels) of semi-diurnal variations over 10° S~10° N based on COSMIC RO observations in 2007. Black lines (left panels) represent 12 monthly mean amplitude profiles whereas phases from the monthly data are shown as open diamond (right panels). The RED thick lines show the annual median values.
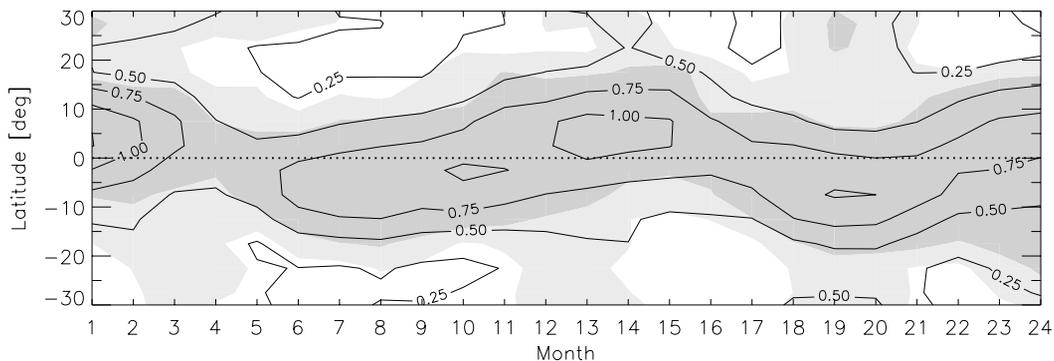
Fig. 3. Amplitudes of the diurnal tide (temperature) at 30 km as a function of latitude (30 S–30 N) and month from COSMIC RO observations (month 1 represents January 2007). The contour interval is 0.25 K. The two-gray-level shaded region denotes the regions where the signal-to-ratio (SNR) of the fitted amplitude are greater than 2 (light gray) and 3 (dark gray), as discussed in Sect. 2.3. Note that almost all amplitudes have SNR>1.
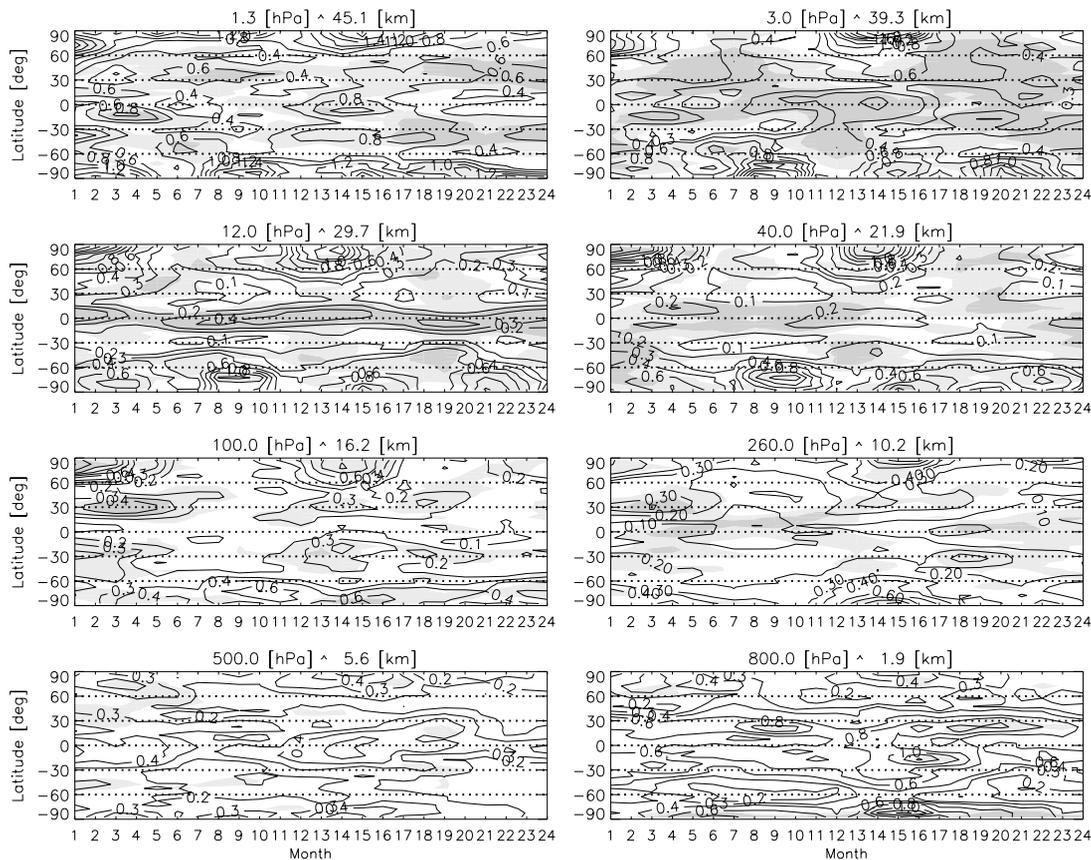
Fig. 4. As in Fig. 3 except for pole-to-pole diurnal amplitude of refractivity in percent at eight pressure levels from 2 km to 45 km.

Title Page

Abstract | Introduction

Conclusions | References

Tables | Figures

◄◄ | ►►

◄ | ►

Back | Close

Full Screen / Esc

Printer-friendly Version

Interactive Discussion
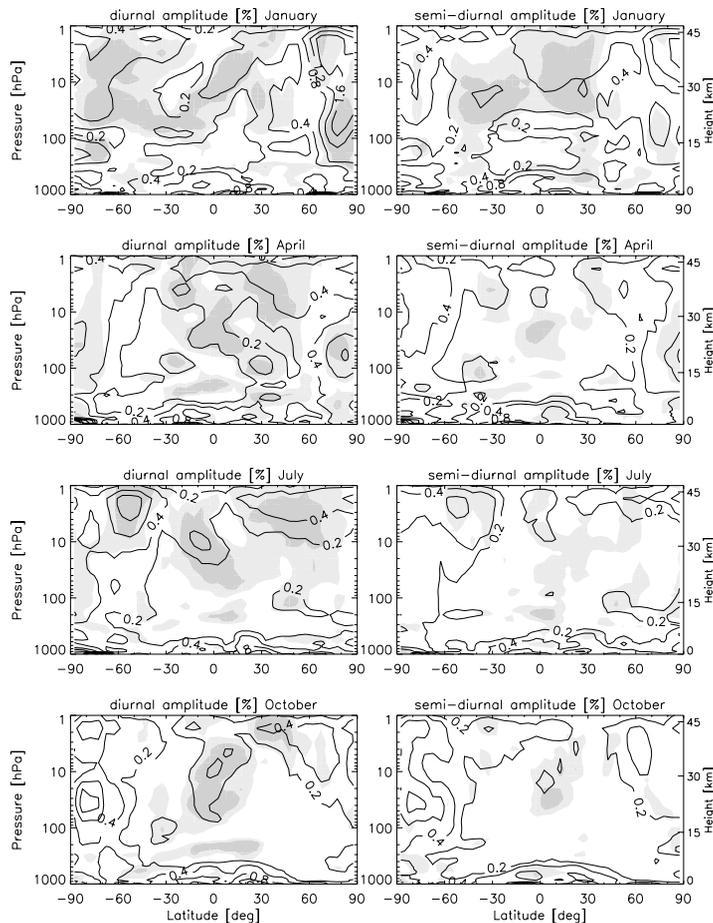
Fig. 5. Vertical structure of zonal mean diurnal (left panels) and semi-diurnal (right panels) refractivity amplitude (in percentage) in four months (January, April, July and October) of year 2007. The definition for the shaded regions is same as in Figs. 3–4.